Microburst Scale Size Distribution Derived with AeroCube-6

M. Shumko[1], T.P. O'Brien[2], J. Sample[1], A. Johnson[1], D.L. Turner[2], J.B. Blake[2], B.A. Griffith[1], O. Agapitov[3], S. Claudepierre[2]

[1]Department of Physics, Montana State University, Bozeman, Montana, USA
[2]Space Science Applications Laboratory, The Aerospace Corportation, El Segundo, California, USA
[3]Space Sciences Laboratory, University of California berkeley, Berkeley, California, USA

Key Points:

- The microburst size distribution in low Earth orbit and the magnetic equator was estimated.
- In low Earth orbit the majority of microbursts have a scale size on the order of a few tens of km.
- At the magnetic equator the size of most microbursts correspond to the scale of highly correlated and high amplitude? whistler-mode chorus waves.

Corresponding author: M. Shumko, `msshumko@gmail.com`

Abstract

Microbursts are an impulsive increase of electrons from the radiation belts into the atmosphere and has been directly observed in low Earth orbit and upper atmosphere. Microburst are believed to be generated by wave-particle scattering between whistler mode waves and radiation belt electrons. Prior work has estimated that microbursts are capable of rapidly depleting the radiation belt electrons on the order of a day, hence their role to radiation belt electron losses must be considered. Radiation belt electron losses due to microbursts is not well understood, and more work is necessary to accurately quantify their contribution. To further address this question we present a statistical study of microburst scale sizes using the pair of AeroCube-6 CubeSats. The microburst scale size distribution in low Earth orbit and the magnetic equator was derived. In low Earth orbit, the majority of microbursts were found to have a size of less than a few tens of km with a minority of microbursts observed at a separation above 50 km. When mapped to the magnetic equator, the microburst scale size distribution corresponds to highly correlated and high amplitude ($> X$ pT) whistler mode chorus scale size derived in prior literature.

1 Plain Language Summary

https://sharingscience.agu.org/creating-plain-language-summary/

2 Introduction

Since the discovery of the Van Allen radiation belts in the 1960s by Van Allen (1959) and Vernov and Chudakov (1960), decades of research has made headway in understanding the dynamics particle acceleration and loss mechanisms. One of acceleration and loss mechanisms extensively studied is wave-particle scattering between whistler-mode chorus waves and electrons (Abel & Thorne, 1998; Meredith et al., 2002; Horne & Thorne, 2003; Thorne et al., 2005; Millan & Thorne, 2007; Bortnik et al., 2008). Whistler-mode chorus waves are typically generated by a temperature anisotropy of low energy electrons up to tens of kiloelectronvolts (keV) and are typically found in the $\sim 6 - 12$ magnetic local times (MLT) (Li, Thorne, Angelopoulos, Bortnik, et al., 2009; Li, Thorne, Angelopoulos, Bonnell, et al., 2009). Whistler-mode chorus waves interact with radiation belt electrons, and are widely believed to cause electron precipitation termed microbursts (Millan & Thorne, 2007)

Microbursts are a subsecond impulse of electrons that are observed by high altitude balloons and satellites in low Earth orbit (LEO) on the radiation belt magnetic footprints, $\sim 4 - 8$ L-shell (L) (Anderson & Milton, 1964; Parks, 1967; Lorentzen, Blake, et al., 2001; Lorentzen, Looper, & Blake, 2001; O'Brien et al., 2003; Woodger et al., 2015; Crew et al., 2016; Breneman et al., 2017; Mozer et al., 2018; Greeley et al., 2019). Microburst's role as a radiation belt electron loss mechanism has been estimated to be significant, with total radiation belt electron depletion due to microbursts estimated to be on the order of a day (Lorentzen, Looper, & Blake, 2001; O'Brien et al., 2004; Thorne et al., 2005; Breneman et al., 2017).

One of the unconstrained microburst parameters that is critical to better quantify the role of microbursts as a loss mechanism is their physical size. Historically there have been various case studies that estimated microburst size. Parks (1967) found that the size of mostly low energy microbursts to be 40±14 km. J. Blake et al. (1996) found a microburst with a size of a few tens of km using the the Solar Anomalous and Magnetospheric Particle Explorer (SAMPEX) and concluded that typically microbursts are less than a few tens of electron gyroradii in size (order of a few km in LEO). Dietrich et al. (2010) also used SAMPEX in another case study and concluded that the observed microbursts were smaller than 4 km. More recently, Crew et al. (2016) used the Focused

Investigation of Relativistic Electron Bursts: Intensity, Range, and Dynamics (FIREBIRD-II) CubeSats and found an example of a microburst larger than 11 km, and Shumko et al. (2018) used FIREBIRD-II to identify a microburst with a size greater than 51 ± 1 km. The large variance in prior results imply that there is a distribution of microburst scale sizes that this study aims to estimate.

Besides addressing the microburst role in radiation belt electron losses, the microburst size distribution is pertinent to identify the wave mode(s) responsible for scattering microbursts. The microburst size distribution in LEO can be mapped to the magnetic equator and the mapped microburst size distribution compared to various wave scales derived in prior literature to identify the dominant wave properties responsible for scattering microburst electrons.

This study addresses these two questions by estimating the microburst size distribution in LEO and the magnetic equator. The twin AeroCube-6 (AC6) CubeSats are utilized for this study because they are ideally equipped for observing microbursts and they took data simultaneously over a span of three years while their separation varied between 2 and 800 km. This paper first describes the AC-6 mission, including their orbit and instrumentation. Then the procedure undertaken to identify microbursts observed by each spacecraft and how they are combined to make a list of the temporally coincident microbursts is described. Next, the microburst size distributions in LEO and the magnetic equator as a function of spacecraft separation is derived. Then a model is developed to understand how various microburst size distributions will be seen by a two-point measurement. Lastly, we discuss and summarize these results and infer the properties of the whistler-mode chorus waves that are believed to cause microbursts.

3 Instrumentation

The AC6 mission consists of a pair of 0.5U (10x10x5 cm) CubeSats built by the Aerospace Corporation and launched on June 19th, 2014 into a 620 x 700 km, 98 degree inclination orbit. The two satellites, designated as AC6-A and AC6-B separated after launch and drifted apart. AC6 has an active attitude control system which allows them to change their differential drag to allow fine separation control. Figure 1a shows the AC6 separation for the duration of the mission.

Each AC6 unit is equipped with a three Aerospace microdosimeters (licensed to Teledyne Microelectronics, Inc). The dosimeter used for this study is dos1 and is identical on both AC6 units. Dos1 has a 30 keV electron threshold and samples at 10 Hz. The AC6 orbit is in the dawn-dusk MLT sectors and Fig. 1b shows the number of quality 10 Hz samples taken simultaneously by AC6 as a function and L and MLT. Quality samples have a 0 data quality flag. The quality flag and detailed technical information on AC6 is described in O'Brien et al. (2016).

4 Methodology

4.1 Microburst Detection

The first step to find microbursts observed simultaneously by both spacecraft is to identify them from each spacecraft separately. We have detected microbursts with two different methods that yielded quantitatively similar results. The first method is the burst parameter (O'Brien et al., 2003). This algorithm has been successfully used in other microburst studies, mainly with the microbursts observed by the Solar Anomalous and Magnetospheric Particle Explorer add citations. For AC6, we found that a burst parameter threshold of 5 has good tradeoff between false positive and false negative microburst detections. Talk about the wavelet based detector as well?

Figure 1. AC6 mission distributions for (a) spacecraft separation and (b) number of simltaneous 10 Hz samples as a function of L and MLT.

The transmitters on AC6 can cause unphysical count impulses in the dosimeters that resembles periodic trains of microbursts. These false detections were removed to remove their bias. One source of transmitter noise was observed at times when AC6 was in contact with the ground stations above mainland US for data downloads and commanding thus the mostly low L detections made above the US were discarded.

Another source of noise is crosslink transmissions between the AC6 units. These transmissions occurred when either spacecraft transitioned from the survey mode to 10 Hz mode. This noise is sometimes not caught by the data quality flag, so the following empirically-derived criteria was developed to remove those detections. The dosimeter with a 250 keV nominal electron threshold, dos2 was used because it had a similar response to noise while rarely responded to microbursts. Since the transmitter noise is very periodic, cross-correlation (CC) and autocorrelation (AC) methods were applied to the dos1 and dos2 time series. Detections were removed if the following two criteria were met: either dos1 or dos2 time series had a AC peak at a 0.2 or 0.4 s lag, and the dos1-dos2 CC was greater than 0.9. The AC lag criteria alone sometimes falsely removed legitimate trains of microbursts, so the second criteria insured that the detection was removed if there was a very high correlation across an order of magnitude in energy.

The lists of microbursts observed by either AC6 unit were merged into a temporally coincident list with the following procedure. Show the microburst detection cartoon I've showed in conferences? The general idea is that a microburst detection on one spacecraft will CC well will the time series from the other spacecraft if it observed a similar microburst, and poorly if there was no microburst observed by the other spacecraft. Each microburst detection made by either spacecraft was CC with the time series from the other spacecraft. Windows of 1 and 1.2 s were used to CC the time series. Different window sizes were used to account for numerical uncertainty due to Poisson noise. Microbursts detections with a CC above 0.8 were considered temporally coincident. This CC threshold was chosen as it is low enough to identify temporally coincident microbursts superposed with noise, and high enough to reject most non-coincident events. Figure 2, panels (a), (c), and (e) show examples of microbursts observed by both AC6 units when they were separated by 6, 17, and 69 km, respectively.

The last CC criteria required that the temporal CC must be greater than the spatial CC + 0.3. The spatial CC was calculated by shifting the AC6-B time series by the in-track lag to CC in latitude. This criteria was applied to remove curtains, spatially stationary and narrow in latitude structures obsered by AC6 (J. B. Blake & O'Brien, 2016) and sometimes appear as microbursts. Figure 2, panels (b), (d), and (f) show the AC6 spatially aligned time series to confirm that the three cases shown were indeed microbursts. The coincident microburst list was then spot checked by two authors to any remove poorly correlated events. Considering the CC criteria and data availability, 662 confirmed simultaneous microburst detections are used to calculate the microburst size distribution in the following section.

4.2 Microburst Size Distribution in LEO and Magnetic Equator

The list of temporally coincident microbursts, which from now on will just be called microbursts, is now compiled to show the fraction of microbursts observed above a separation s. When AC6 observes a microburst at s, the microburst's size must be greater than s. This fact, along with the arguments presented in Section 4 in Joy et al. (2002), is used to investigate the dependence of the number of microbursts observed above s, as a function of s which is the microburst complementary cumulative distribution $F(s)$.

Include the following Bayes theorem proof? It does not seem necessary (or I did not motivate it) If P(A) is the probability that a microburst is larger than s and P(B) is the probability that AC6 is separated by s, then the fraction of microbursts observed

Figure 2. Examples of microbursts observed simultaneously by AC6. Panels (a), (c) and (e) shows the temporally-aligned time series at spacecraft separations of 5.6 km, 16.5 km, and 68.5 km, respectively. Panels (b), (d), and (f) show the spatially aligned time series corresponding to the time series in the same column. The clear temporal correlation and lack of spatial correlation demonstrates that these events are microbursts.

at s is the conditional probability $P(A \mid B)$. Using Bayes theorem,

$$P(A \mid B) = \frac{P(A \ \& \ B)}{P(B)} \tag{1}$$

where $P(A \ \& \ B)$ is the joint probability. Since the AC6 separation is independent of microburst size, $P(A \ \& \ B) = P(A)P(B)$. Hence

$$P(A \mid B) = \frac{P(A)P(B)}{P(B)} = P(A) \tag{2}$$

so AC6 is observing the probability that the microburst is larger than s.

The cumulative number of microbursts observed above s is the ratio of $N(s)$, the number of microbursts observed above s to $N(0)$, the total number of microbursts observed

$$F(s) = \frac{N(s)}{N(0)} \tag{3}$$

$$N(s) = \sum_{i=s}^{\infty} n_i \frac{S_{max}}{S_i} \tag{4}$$

where n_i is the number of microbursts observed by AC6 in ith bin. The normalization term S_{max}/S_i is a ratio of the number of samples observed in the most sampled bin to the number of samples in ith bin. This normalization factor corrects for AC6's non-uniform sampling in separation and the number of samples is shown in Fig. 3c. With this normalization, $F(s)$ can be interpreted as the fraction of microbursts observed above s assuming AC6 sampled evenly in separation. Microburst $F(s)$ in LEO is shown by the black curve in Fig. 3a for $4 < L < 8$ and split into one L-wide bins with the colored curves. The separation bin width used in Fig. 3 is 5 km. To check for bias in $F(s)$ due to the separation bins, $F(s)$ was resampled with other bin widths and offsets. Bin widths as large as the size of the features in $F(s)$ ($20 - 30$ km) and bin offsets up to 50% of the bin width did not qualitatively effect the curves in Fig. 3a.

The overall trend in Fig. 3a consists of a sudden cumulative probability drop off, followed by a shoulder up to $s \approx 70$ km where the cumulative distribution drops to nearly zero. The shaded region around the black curve shows the standard error due to counting statistics. The uncertainty due to false coincidence events i.e. two unrelated microbursts

randomly lining up in time was also considered. The microburst duty cycle in a one minute window ($\approx 1\ L$) around each microburst was calculated. The false coincidence probability is the square of the duty cycle and was found to be less than 5% for the majority of microbursts. The false coincidence probability for each microburst was then used to randomly remove microbursts and $F(s)$ was recalculated in 1000 trials. The uncertainty in $F(s)$ with microbursts randomly removed was much smaller than the uncertainty due to counting statistics alone. Lastly, Fig. 3b shows the microburst probability density (PD), calculated by differentiating $F(s)$, and shows a peak at $s < 20$ km as well as a peak between 70-80 km separation.

To compare the microburst size to the size of their progenitor waves, the spacecraft locations during observed microbursts were mapped to the magnetic equator using the Olson-Pfitzer magnetic field model (Olson & Pfitzer, 1982) which is implemented with a Python wrapper for IRBEM-Lib (Boscher et al., 2012). As previously stated, a microburst observed in LEO has a size larger than the spacecraft separation, hence that microburst would also have a size larger than the spacecraft separation after it was mapped to the magnetic equator. Thus the procedure to estimate $F(s)$ is identical to the LEO size distribution but with a different normalization. The normalization factors were calculated by mapping every quality AC6 sample taken simultaneously to the magnetic equator and binning them by equatorial separation into 100 km bins. Figure 4 shows the equatorial microburst size distribution in the same format as Fig. 3. Similar to the microburst PD in LEO, most of the equatorial microburst PD was observed when the AC6 equatorial separation was less than 300 km.

The results in Figs. 3 and 4 show the fraction of microbursts observed above a spacecraft separation and do not fully represent the microbursts size distribution due to the compounding effects from the range of microburst sizes and random locations of microbursts with respect to AC6 i.e. even if the microburst size is much larger than s, a fraction of those microbursts will graze only one AC6 unit and not be observed by the other. Thus modeling is necessary to capture the compounding influence of these statistical effects on AC6, a two-point measurement.

5 Modeling the Distribution of Microburst Sizes

5.1 Monte Carlo and Analytic Models to Estimate $F(s)$

TO-DO

- Show a LEO CDF model assuming a fixed-sized microburst population.
- Decide if I should show a two-fixed-sized microburst population or a microburst CDF.
- Show the residuals in the plots.
- Think about a model comparison.

To account for the effects due to microbursts randomly occurring in the vicinity of AC6 with an unknown distribution of microburst sizes, Monte Carlo (MC) and analytic models were developed. These models assume a hypothesized distribution of microburst sizes expressed with a probability density function $P(r)$, and a microburst geometry to estimate $F(s)$. Microbursts are assumed to be circular with a radius r. A few distribution of microburst size hypotheses are considered: a one-size microburst population, a two-size microburst population, and X continuous $P(r)$.

The MC model is the most intuitive to understand and it consists of randomly scattering 10^5 microburst centers in a 400 x 400 km grid around AC6 of various r that are distributed according to $P(r)$. Spacecraft A is placed at the origin, and spacecraft B is placed along the positive y-axis at predetermined distances from the origin correspond-

Figure 3. Fraction of microbursts greater than the spacecraft separation as a function of separation in LEO. Panel (a) shows the fraction of microbursts observed above that separation. Panel (b) shows the microburst probability density as a function of separation. Lastly, panel (c) shows the number of simultaneous samples AC6 observed as a function of separation. The colored lines show the distributions binned by L, and the thick black curve shows the fraction of microbursts observed above a separation in the entire radiation belt ($4 < L < 8$). The gray shading around the black curve shows the uncertainty due to counting statistics.

Figure 4. Microburst scale size distribution in the same format as Fig. 3 and mapped to the magnetic equator.

ing to he AC6 separation bins used in Section 4.2 Then the cumulative number of simultaneously observed microbursts at spacecraft A and each spacecraft B location was counted. The modeled fraction of microbursts observed above s is then

$$F(s) = \frac{\sum\limits_{i>s}^{\infty} n_i}{\sum\limits_{i>0}^{\infty} n_i}.$$
(5)

where as before the number of microbursts observed by both spacecraft in ith bin is n_i.

The analytic model, while identical to the MC model, highlights the geometrical concepts connecting the microburst size distribution and $F(s)$. Assuming that microbursts are circular with radius r and AC6 are separated by s, there is an area where a microburst will be observed by both spacecraft. Figure 5a shows this geometry with the two spacecraft indicated with the black dots. All microbursts who's center lies inside the circular area of radius r that surrounds the top spacecraft will be observed by the top spacecraft. Likewise the same argument applies to the bottom spacecraft. The intersection of these two areas defines another area, $A(r, s)$ where a microburst will be observed by both spacecraft and is given by the circle-circle intersection area equation,

$$A(r, d) = 2r^2 \cos^{-1}\left(\frac{d}{2r}\right) - \frac{d}{2}\sqrt{4r^2 - d^2}.$$
(6)

Cite anything? Wolfram: http://mathworld.wolfram.com/Circle-CircleIntersection.html
Example geometries with an overlapping area are shown in Fig. 5b, c.

The circle intersection area can be thought of as a probability that a microburst will be observed by both spacecraft, given that it was observed by one. The hypothesized $P(r)$ can be thought of as the relative occurrence of microbursts at various r and is effectively a weighting factor on $A(r, s)$ which is integrated out (marginalized) since AC6 is observing the overall effect of microbursts at all r. Lastly, a cumulative integral over a dummy variable s' is applied to the normalized areas to calculate $F(s)$. With these considerations the analytic $F(s)$ is given by

$$F(s) = \frac{\int\limits_{s}^{\infty}\int\limits_{0}^{\infty} A(r, s')P(r)drds'}{\int\limits_{0}^{\infty}\int\limits_{0}^{\infty} A(r, s')P(r)drds'}.$$
(7)

where as in the MC model the denominator is the normalization factor. To illustrate the effects of random microburst locations around AC6, example analytic and MC model $F(s)$ assuming a fixed-size 40 km diameter microburst population is shown in Fig. 5d with the dashed blue and red curves, respectively.

5.2 Estimating optimal parameters for microburst size models

At this stage the microburst models are used with a few hypothesized microburst size distributions to estimate the optimal set of distribution parameters. To estimate the optimal model parameters given the AC6 data, a Bayesian approach was taken using a Metropolis Markov Chain Monte Carlo (MCMC) sampler. This MCMC sampler samples the model parameter space under the following assumptions. First assumption is prior knowledge of model parameters which is called a prior and mathematically expressed with a probability density function (PDF). For the MC microburst size model uniformly and normally distributed priors are assumed. The second assumption is the likelihood
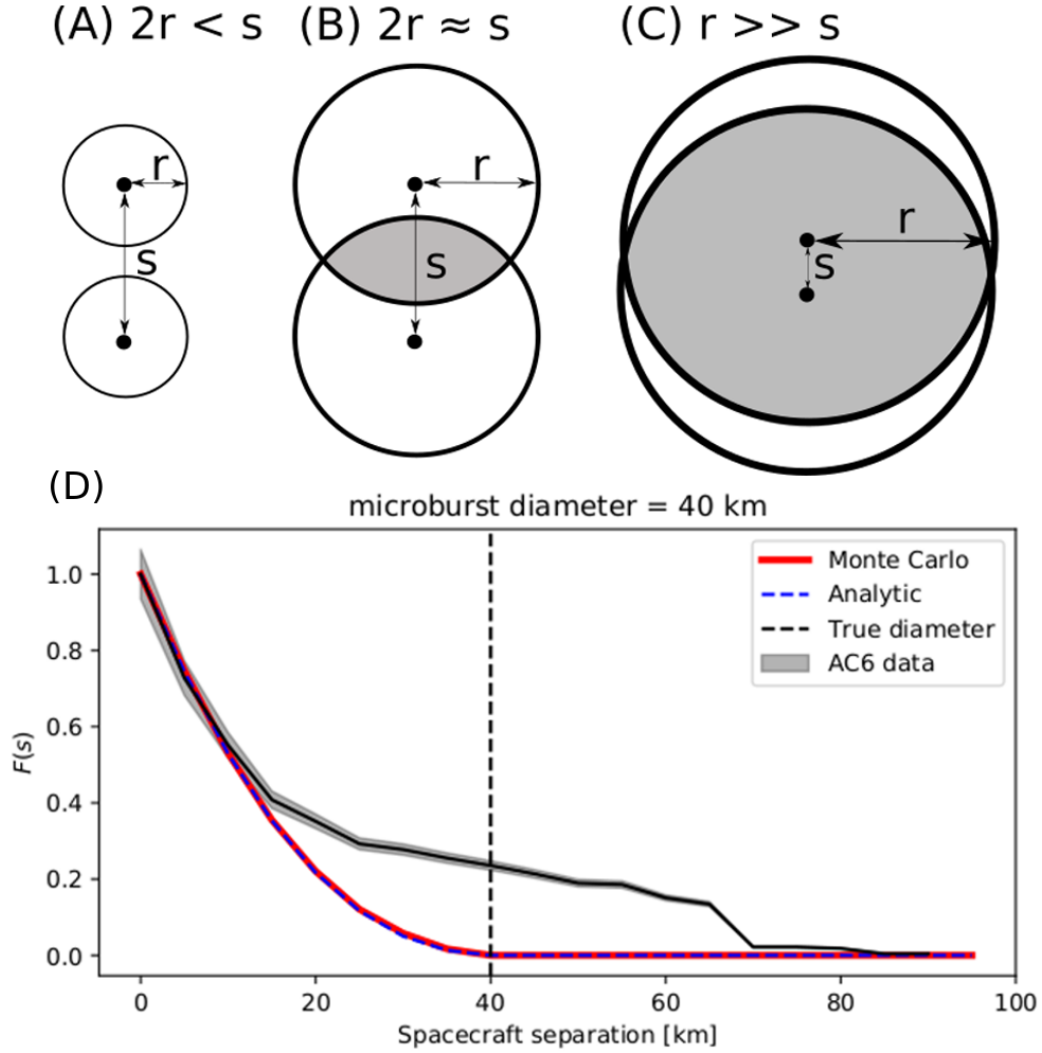
Figure 5. Panels A-C show the geometry of the analytic model. The two spacecraft are shown as black dots. The enclosing black circle around each spacecraft bounds the area where a microburst will be observed by one or both AC6 units if the microburst's center lies inside the circle. Panel (A) shows the case where microburst diameter is smaller than the AC6 separation and all microbursts will be observed by either unit A or B and never simultaneously. Panel (B) shows the intermediate case where the microburst diameter is comparable to the AC6 separation and some fraction of microbursts will be observed simultaneously. The fraction of the microbursts simultaneously observed is proportional to the circle intersection area shown with grey shading. Panel (C) shows the case where the spacecraft separation is much smaller than the microburst size and nearly all microbursts will be observed by both spacecraft. Lastly panel (D) shows $F(s)$ from the AC6 data with a solid black line, and a MC and analytic $F(s)$ for a single-sized microburst distribution with a 40 km diameter.

function that is the probability of observed data given the model parameters. With these two assumptions the MCMC sampler iterates N times, each time picking a random set prior parameters for that particular microburst PDF. For each set of prior parameters, their prior probability is weighted by the likelihood to calculate the probability that the current set of prior parameters is explained by the data. With the Metropolis sampler, the random prior parameters are sampled in a way that is weighted by the prior and likelihood and mostly explores the regions of parameter space that is more probable.

After N trails the tested parameters as a function of trial is called a trace and the histogram of the trace is the posterior probability density of that model parameter.

6 Discussion

TO-DO

- Discuss the significance of the peaks in the LEO CDF & PDF.
- Discuss the secondary peak.
- Talk about how these sizes fit in with prior work and how they can be used to estimate microburst loss rates.
- Maybe add a plot with Oleksiy's data?
- Use the wave data to interpret the equatorial scale size distribution. Is the ¡ 200 km peak due to high amplitude waves, or is it just that waves are most common at those scales?

7 Conclusions

References

Abel, B., & Thorne, R. M. (1998). Electron scattering loss in earth's inner magnetosphere: 1. dominant physical processes. *Journal of Geophysical Research: Space Physics*, *103*(A2), 2385–2396.

Anderson, K. A., & Milton, D. W. (1964). Balloon observations of X rays in the auroral zone: 3. High time resolution studies. *Journal of Geophysical Research*, *69*(21), 4457–4479. Retrieved from `http://dx.doi.org/10.1029/JZ069i021p04457` doi: 10.1029/JZ069i021p04457

Blake, J., Looper, M., Baker, D., Nakamura, R., Klecker, B., & Hovestadt, D. (1996). New high temporal and spatial resolution measurements by sampex of the precipitation of relativistic electrons. *Advances in Space Research*, *18*(8), 171 - 186. Retrieved from `http://www.sciencedirect.com/science/article/pii/0273117795009698` doi: http://dx.doi.org/10.1016/0273-1177(95)00969-8

Blake, J. B., & O'Brien, T. P. (2016). Observations of small-scale latitudinal structure in energetic electron precipitation. *Journal of Geophysical Research: Space Physics*, *121*(4), 3031–3035. Retrieved from `http://dx.doi.org/10.1002/2015JA021815` (2015JA021815) doi: 10.1002/2015JA021815

Bortnik, J., Thorne, R., & Inan, U. S. (2008). Nonlinear interaction of energetic electrons with large amplitude chorus. *Geophysical Research Letters*, *35*(21).

Boscher, D., Bourdarie, S., O'Brien, P., Guild, T., & Shumko, M. (2012). *Irbem-lib library.*

Breneman, A., Crew, A., Sample, J., Klumpar, D., Johnson, A., Agapitov, O., ...

others   (2017).   Observations directly linking relativistic electron microbursts to whistler mode chorus: Van allen probes and FIREBIRD II.   *Geophysical Research Letters*.

Crew, A. B., Spence, H. E., Blake, J. B., Klumpar, D. M., Larsen, B. A., O'Brien, T. P., ... Widholm, M.   (2016).   First multipoint in situ observations of electron microbursts: Initial results from the NSF FIREBIRD II mission.   *Journal of Geophysical Research: Space Physics*, *121*(6), 5272–5283.   Retrieved from `http://dx.doi.org/10.1002/2016JA022485`   (2016JA022485)   doi: 10.1002/2016JA022485

Dietrich, S., Rodger, C. J., Clilverd, M. A., Bortnik, J., & Raita, T.   (2010).   Relativistic microburst storm characteristics: Combined satellite and ground-based observations. *Journal of Geophysical Research: Space Physics*, *115*(A12).

Greeley, A., Kanekal, S., Baker, D., Klecker, B., & Schiller, Q.   (2019).   Quantifying the contribution of microbursts to global electron loss in the radiation belts. *Journal of Geophysical Research: Space Physics*.

Horne, R. B., & Thorne, R. M.   (2003).   Relativistic electron acceleration and precipitation during resonant interactions with whistler-mode chorus.   *Geophysical Research Letters*, *30*(10).   Retrieved from `http://dx.doi.org/10.1029/2003GL016973`   (1527) doi: 10.1029/2003GL016973

Joy, S., Kivelson, M., Walker, R., Khurana, K., Russell, C., & Ogino, T.   (2002).   Probabilistic models of the jovian magnetopause and bow shock locations. *Journal of Geophysical Research: Space Physics*, *107*(A10), SMP–17.

Li, W., Thorne, R., Angelopoulos, V., Bonnell, J., McFadden, J., Carlson, C., ... Auster, H.   (2009).   Evaluation of whistler-mode chorus intensification on the nightside during an injection event observed on the THEMIS spacecraft. *Journal of Geophysical Research: Space Physics*, *114*(A1).

Li, W., Thorne, R. M., Angelopoulos, V., Bortnik, J., Cully, C. M., Ni, B., ... Magnes, W.   (2009).   Global distribution of whistler-mode chorus waves observed on the THEMIS spacecraft.   *Geophysical Research Letters*, *36*(9).   Retrieved from `http://dx.doi.org/10.1029/2009GL037595`   (L09104)   doi: 10.1029/2009GL037595

Lorentzen, K. R., Blake, J. B., Inan, U. S., & Bortnik, J.   (2001).   Observations of relativistic electron microbursts in association with VLF chorus.   *Journal of Geophysical Research: Space Physics*, *106*(A4), 6017–6027.   Retrieved from `http://dx.doi.org/10.1029/2000JA003018` doi: 10.1029/2000JA003018

Lorentzen, K. R., Looper, M. D., & Blake, J. B.   (2001).   Relativistic electron microbursts during the GEM storms.   *Geophysical Research Letters*, *28*(13), 2573–2576.   Retrieved from `http://dx.doi.org/10.1029/2001GL012926` doi: 10.1029/2001GL012926

Meredith, N., Horne, R., Summers, D., Thorne, R., Iles, R., Heynderickx, D., & Anderson, R.   (2002).   Evidence for acceleration of outer zone electrons to relativistic energies by whistler mode chorus.   In *Annales geophysicae* (Vol. 20, pp. 967–979).

Millan, R., & Thorne, R.   (2007).   Review of radiation belt relativistic electron losses.   *Journal of Atmospheric and Solar-Terrestrial Physics*, *69*(3), 362 - 377.   Retrieved from `//www.sciencedirect.com/science/article/pii/S1364682606002768` doi: http://dx.doi.org/10.1016/j.jastp.2006.06.019

Mozer, F. S., Agapitov, O. V., Blake, J. B., & Vasko, I. Y.   (2018).   Simultaneous observations of lower band chorus emissions at the equator and microburst precipitating electrons in the ionosphere.   *Geophysical Research Letters*.   Retrieved from `http://dx.doi.org/10.1002/2017GL076120`   doi: 10.1002/2017GL076120

O'Brien, T. P., Blake, J. B., & W., G. J.   (2016, May).   *Aerocube-6 dosimeter data readme* (Tech. Rep. No. TOR-2016-01155). The Aerospace Corporation.

O'Brien, T. P., Looper, M. D., & Blake, J. B.   (2004).   Quantification of relativis-

tic electron microburst losses during the GEM storms. *Geophysical Research Letters*, *31*(4). Retrieved from `http://dx.doi.org/10.1029/2003GL018621` (L04802) doi: 10.1029/2003GL018621

O'Brien, T. P., Lorentzen, K. R., Mann, I. R., Meredith, N. P., Blake, J. B., Fennell, J. F., . . . Anderson, R. R. (2003). Energization of relativistic electrons in the presence of ULF power and MeV microbursts: Evidence for dual ULF and VLF acceleration. *Journal of Geophysical Research: Space Physics*, *108*(A8). Retrieved from `http://dx.doi.org/10.1029/2002JA009784` doi: 10.1029/2002JA009784

Olson, W. P., & Pfitzer, K. A. (1982). A dynamic model of the magnetospheric magnetic and electric fields for july 29, 1977. *Journal of Geophysical Research: Space Physics*, *87*(A8), 5943–5948. Retrieved from `http://dx.doi.org/10.1029/JA087iA08p05943` doi: 10.1029/JA087iA08p05943

Parks, G. K. (1967). Spatial characteristics of auroral-zone X-ray microbursts. *Journal of Geophysical Research*, *72*(1), 215–226.

Shumko, M., Sample, J., Johnson, A., Blake, B., Crew, A., Spence, H., . . . Handley, M. (2018). Microburst scale size derived from multiple bounces of a microburst simultaneously observed with the firebird-ii cubesats. *Geophysical Research Letters*, *45*(17), 8811-8818. Retrieved from `https://agupubs.onlinelibrary.wiley.com/doi/abs/10.1029/2018GL078925` doi: 10.1029/2018GL078925

Thorne, R. M., O'Brien, T. P., Shprits, Y. Y., Summers, D., & Horne, R. B. (2005). Timescale for MeV electron microburst loss during geomagnetic storms. *Journal of Geophysical Research: Space Physics*, *110*(A9). Retrieved from `http://dx.doi.org/10.1029/2004JA010882` (A09202) doi: 10.1029/2004JA010882

Van Allen, J. A. (1959). The geomagnetically trapped corpuscular radiation. *Journal of Geophysical Research*, *64*(11), 1683–1689. Retrieved from `http://dx.doi.org/10.1029/JZ064i011p01683` doi: 10.1029/JZ064i011p01683

Vernov, S., & Chudakov, A. (1960). Investigation of radiation in outer space. In *International cosmic ray conference* (Vol. 3, p. 19).

Woodger, L., Halford, A., Millan, R., McCarthy, M., Smith, D., Bowers, G., . . . Liang, X. (2015). A summary of the BARREL campaigns: Technique for studying electron precipitation. *Journal of Geophysical Research: Space Physics*, *120*(6), 4922–4935.